Formation and chemical properties of nanostructured bimetallic surfaces

Harry E. Hoster[1], Andreas Bergbreiter[1], Otávio B. Alves[1], R. Jürgen Behm[1], Axel Groß[2]

[1] Institut für Oberflächenchemie und Katalyse, Universität Ulm, D-89081 Ulm, Germany
[2] Institut für Theoretische Chemie, Universität Ulm, D-89081 Ulm, Germany

Summary

We report on the structure, formation, and stability of nanostructured bimetallic surfaces. These surfaces are used to study selected aspects of the structure-activity relationships in electrochemistry and electrocatalysis, with a special focus on electronic and geometric effects on the (sub-)nm scale. The results are based on a close cooperation between experiment and theory, specifically, on adsorption and reaction experiments at nanostructured bimetallic surfaces and on density functional calculations of metal-metal and adsorbate-metal interactions.

As model systems, we have chosen Pt(111), Pd(111), and Ru(0001) single crystal surfaces, which were modified by vapor deposition of different foreign metals (Au, Ag, Pt, Pd, Ru) and optional sample heating. The resulting nanostructures are divided into (A) island morphologies, (B) mono- and multilayer films, and (C) monoatomically thin surface alloys. Type and availability of the different chemically relevant structure elements were determined from quantitatively evaluated scanning tunnelling microscopy (STM) data. For the surface alloys, we succeeded in simulating the atom distribution using a Monte-Carlo approach based on pairwise metal-metal interactions. The necessary interaction parameters could either be approximated from experimental results by systematic variation towards an optimum agreement between simulated and measured atom distribution, or by fitting to density functional theory data. The experiments also focussed on the nm-scale processes during the formation of surface alloys. For selected systems, we could furthermore show that thermodynamically the surface alloys reflect a local equilibrium and thus are metastable against loss of the foreign metal by bulk diffusion when the temperature is kept below a certain threshold.

The (electro-)chemical properties of the different model systems were studied by thermal desorption experiments in vacuum on the one hand and by cyclic voltammetry in electrolyte on the other. Experiments and density functional calculations concordantly show that the local adsorption properties can be systematically varied via the thickness of the foreign metal film, or via the composition of the surface alloys. This can be rationalized via the interplay of electronic vertical ligand and strain-effects, and by mixed ensemble and (lateral) ligand effects, respectively. As an example, we highlight the importance of sub-nm scale atomic dispersion for the electrocatalytic activity of PtRu electrodes towards CO oxidation. In total, our studies not only promote the understanding of nanostructure formation at bimetallic surfaces, but also reveal promising pathways for a systematic tuning of these surfaces with respect to their electrocatalytic reactivities.

For publication in: Functional Nanostructures II, Springer Series *Nanoscience & Technology,* T. Schimmel and H. v. Löhneysen, Eds. (Springer-Verlag, Berlin – Heidelberg - New York – Tokyo, 2010).

1 Introduction

The use of bimetallic alloys as electrode materials is a promising approach for an improvement of their electrocatalytic activity [1,2]. The rates and the selectivities of reactions at these electrodes depend sensitively on their composition and nanostructure. As in heterogeneous catalysis, the interplay of a number of electronic and geometric effects has to be considered. Most important are variations in the local adsorption properties due to changes in the electronic structure, which often result from compression or expansion of the crystal lattice (strain effects) [3-6] or from the intermetallic bonds in the (near-)surface region (ligand effects) [2,7]. Another important aspect is the space requirement for adsorbed species in the distinct elementary steps of the surface reactions, which is referred to as geometric ensemble effect [2,7-9]. Reaction paths with a larger space requirement for adsorbed reactants or intermediates can be suppressed by mixtures of active and inactive metals, thus increasing the selectivity towards pathways with lower space requirement. Apart from the adsorption properties for individual species, many reactions require sites for two different reactants in direct vicinity, e.g., for a Langmuir-type reaction mechanism. On a bimetallic surface, the different reactants may be specifically stabilized by different sites (bifunctional mechanism)

On real bimetallic surfaces, these effects usually occur simultaneously. In recent years, advances in the theoretical and experimental methods have increasingly improved the understanding of the separate phenomena themselves and also their interplay. Though technically applicable electrocatalysts usually consist of small particles, many important insights are derived in studies at planar model systems. Three generic types of bimetallic particles and corresponding planar model systems are assembled in Fig. 1.

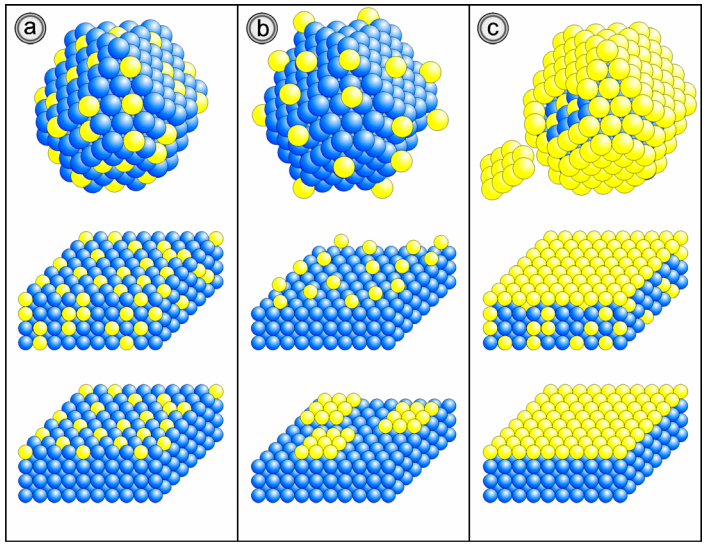

Fig. 1. Bimetallic nanoparticles and corresponding planar model systems; a) alloy particle (top), bulk alloy surface (middle), surface confined alloy (bottom); b) admetal modified particle (top), admetal modified single crystal (middle), island modified single crystal (bottom); c) alloy particle covered by a shell of one component (top), bulk alloy covered by a monolayer of one component (middle), single crystal covered by an atomically smooth adlayer (bottom).

High-resolution scanning tunneling microscopy (STM) with chemical contrast [10,11] provides direct information about the distribution of the metallic components within the surface. Through variations of the (local) surface structure and composition, and its correlation with the (integrated) chemical/catalytic properties, it was possible to derive adsorption and catalytic properties for single surface nanostructures [12-14]. Likewise, advances in computing performance and the development of effective algorithms now allow

quantitative predictions on the chemical properties of real bimetallic systems based on electronic structure theory from first principles, i.e., without empiric parameters [3-6,15,16]. Such predictions comprise the role of strain and ensemble effects on adsorption energies and reaction barriers of bimetallic catalysts [3-6,12,14].

Particularly successful are usually studies where theoretical and experimental methods focus on the same model system [4,14]. Such studies require a high agreement between composition and nanostructure of the systems considered in experiments and calculations. The research thus splits into two main sections, which concern (i) the structure and stability of the model systems and (ii) their (electro-)chemical properties. This is reflected in the structure of this chapter. Using Pt_xRu_{1-x}/Ru(0001) as example, we will highlight some important aspects of the formation of A_xB_{1-x}/B (A=foreign metal, B=substrate) surface alloys, which form a particularly interesting class of nanostructured model systems. Related to this, we will show some results that underline the stability of the surface alloy as a metastable phase: even after being covered by a thin layer of the substrate metal (Ru), the surface alloy recovers after heating to a suitable temperature. We will also demonstrate that depending on the metal combination also the opposite case may occur, where the foreign metal is preferably buried in the subsurface region. Apart from the surface confinement and the stability of a surface alloys, it is the lateral distribution of the metals A and B that is most important for the understanding of their (electro-)chemical properties. We therefore quantitatively analyse the atom distribution for different A-B combinations and compare the results to the corresponding ab-initio predictions [17,18]. On the other hand, we will demonstrate the kind of information about the structure determining metal-metal interactions that can be directly derived from the atom distributions analysed by STM. For the system Pt_xAu_{1-x}/Pt(111), we will give an example, how the nanostructure and the adsorption properties can be predicted by ab-initio methods in combination with Monte-Carlo (MC) simulations, and how these results fit to the corresponding experiments. In the last section, we will highlight the direct influence of the nanostucture of a bimetallic PtRu surface on its electrocatalytic activity towards CO oxidation.

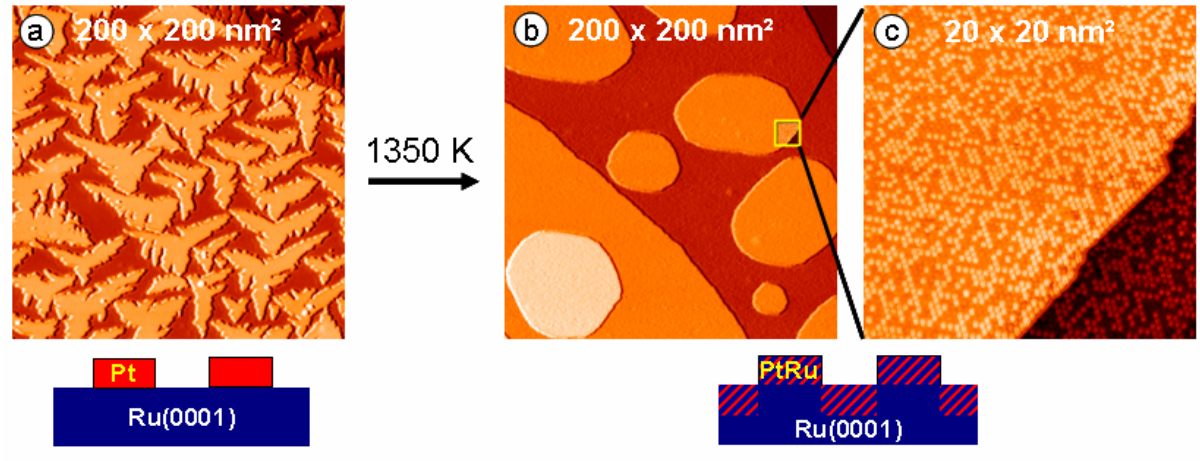

Fig. 2 a) Ru(0001) surface after deposition of 0.5 ML Pt at 300 K. b) The same surface after annealing to 1350 K. c) Atomically resolved image of an island edge (see frame marked in (b)) showing 50% Pt atoms (dark due to chemical contrast) on the island and the surrounding terrace. Reproduced with permission from ref. [19].

2 Results and Discussion

2.1 Surface alloy formation

Vapor deposition of Pt onto Ru(0001) at 300 K leads to the formation of triangular Pt islands with a height of one atomic layer (see Fig. 2a). Heating such a surface to temperatures $T \geq 850$ K causes Pt-Ru intermixing, and brief annealing to 1300 - 1350 K results in the formation of atomically dispersed monolayer surface alloys with an essentially random distribution of the two components in the surface layer (see atomic resolution STM images in Fig. 2c and in refs. [19,19-21]). Based on quantitative STM measurements, the loss of Pt into deeper layers is negligible up to Pt surface contents of 0.8 under these conditions, and less than 10% up to 1 ML Pt predeposition (see Fig. 3) [19]. This can be rationalized by a highly negative surface segregation energy of Pt impurities in Ru [17,18], in combination with a barrier for Pt diffusion into deeper Ru regions, which must be significantly higher than that for Pt exchange with Ru surface atoms.

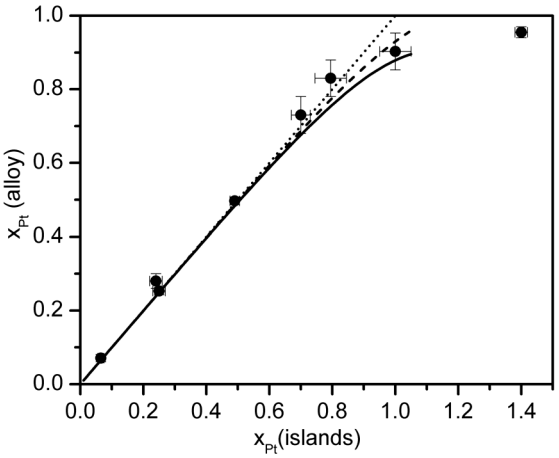

Fig. 3 Pt content counted in the surface alloys as a function of initial Pt coverage. Dotted line: no Pt loss; dashed/solid line: quasi-equilibrium of the Pt contents in the two outermost layers as calculated from ab-initio segregation energies [17,18]. Reproduced with permission from ref. [19]

In combination with surface diffusion, such place exchange processs are sufficient to explain the process of surface alloy formation, as we have illustrated in Fig. 4. At sufficiently high temperature, Pt adatoms detach from the Pt islands and diffuse over the Ru lattice (Fig. 4a). They have a certain probability for place exchange with atoms in the underlying layer, which in the beginning are mostly Ru. The Ru atoms can then attach to the Pt islands. As illustrated in Fig. 4b, we propose that the islands preferentially overgrow areas without incorporated Pt atoms. This can be rationalized by the higher binding energy of both Pt and Ru to underlying Ru than to Pt atoms. Hence, Pt atoms in the terrace remain exposed and thus have a high probability to become re-replaced by Ru atoms. In total, this leads to an island morphology without buried Pt atoms, and thus to the identical composition on the islands and the surrounding terraces as observed in the atomically resolved STM analyses (see Figs. 2b and 2c).

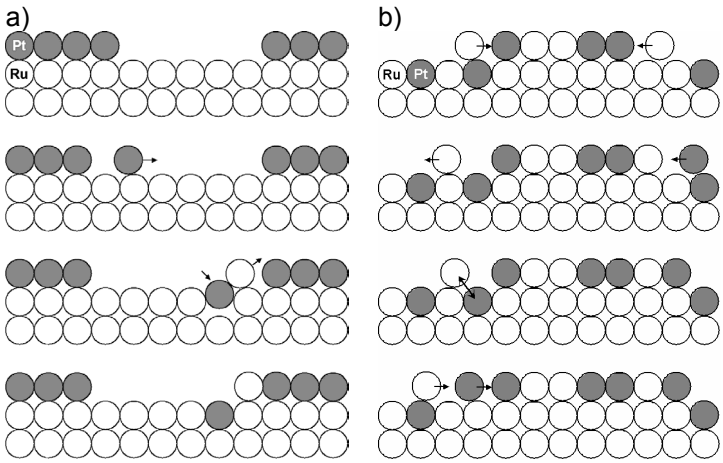

Fig. 4 a) Adatom mediated exchange between islands and surrounding terrace areas. b) Reversible exchange of Pt atoms upon overgrowth by an island, resulting in growth of islands over Pt-free areas. Reproduced with permission from ref. [19]

2.2 Stability of surface alloys

The interplay between metal-metal interactions, surface diffusion and exchange processes described above should also lead to a re-exposition of foreign metal atoms that have been deliberately overgrown by islands of the host (or substrate) metal. For the systems Pt_xRu_{1-x}/Ru(0001) and Pd_xRu_{1-x}/Ru(0001), this could indeed be experimentally confirmed. For the latter system, the resulting sequence of surface morphologies is assembled in Fig. 5. A $Pd_{44}Ru_{56}$/Ru(0001) surface alloy is formed by vapor deposition of 0.44 ML Pd onto Ru(0001) (Fig. 5a), followed by annealing at 1150 K for 10 s. The island morphology disappears (Fig. 5b), and atomically resolved STM images (Fig. 5c) show the formation of a surface confined alloy with 44 % dark (= Pd) and 56 % bright (= Ru) atoms [22,23]. This surface was subsequently covered by 1.2 atomic layers of vapor deposited Ru (see Fig. 5d), and then heated again to 1150 K for 10 s. As shown in Figs. 5e and 5f, the surface morphology, composition and nm-scale atom distribution is similar to that of the initially formed surface alloy. This underlines that the surface alloy indeed reflects a local equilibrium structure with a considerable stability against small perturbations. Furthermore, the initial island morphologies (Figs. 2a and 5a) are metastable against surface alloy formation. Some aspects about the underlying driving forces will be elucidated in the following paragraph.

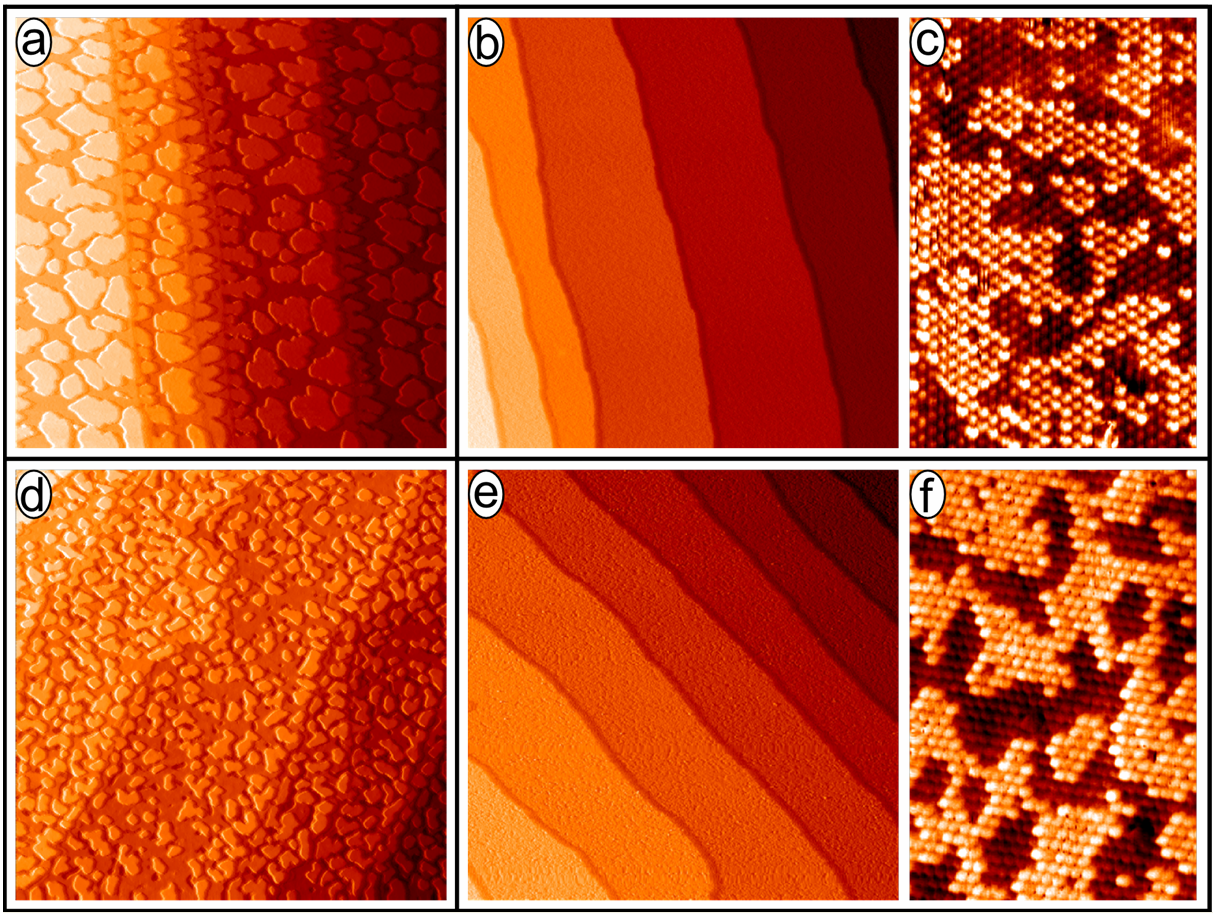

Fig. 5. STM images illustrating the floating of a Pd_xRu_{1-x}/Ru(0001) surface alloy. a) 0.44 ML Pd deposited on Ru(0001) at 300K (200 x 200 nm²). b) Surface morphology (200 x 200 nm²) after annealing to 1150 K for 10 s. c) Atomic resolution image with chemical contrast (6 x 9 nm²) of the surface in b), showing the formation of a $Pd_{44}Ru_{56}$/Ru(0001) surface alloy (dark / bright atoms = Pd / Ru). d) Surface morphology (200 x 200 nm²) after overgrowth of the surface alloy by 1.2 ML Ru at 500K. e) Surface morphology (200 x 200 nm²) after annealing to 1150 K. f) Atomic resolution image with chemical contrast (6 x 9 nm²), showing the re-formation of a $Pd_{44}Ru_{56}$/Ru(0001) surface alloy. Reproduced with permission from ref. [24]

A complementary behavior can be expected when the impurity segregation energy of the guest in the host metal is not negative but positive [17,18]. As an example, we have studied the temperature dependent growth of Ru on Pt(111) [25,26]. An overview about the results is shown in Fig. 6. At temperatures below 523 K, Ru forms islands with a preferred height of two atomic layers. This results from the higher bonding strength of Ru monolayer islands due to their direct contact to the less strongly binding Pt substrate, which stabilizes Ru atoms on top of Ru monolayer islands compared to Pt(111), or on Ru islands with greater thickness [26]. As illustrated in Figs. 6e-6h, those bilayer islands vanish when surface alloy formation becomes kinetically possible. The onset of surface alloying is accompanied by an overgrowth of the Ru-rich surface alloys by Pt-rich ones. Auger electron spectroscopy measurements indicate that the majority of the Ru atoms stay in the near-surface region in the temperature range up to 773 K [25].

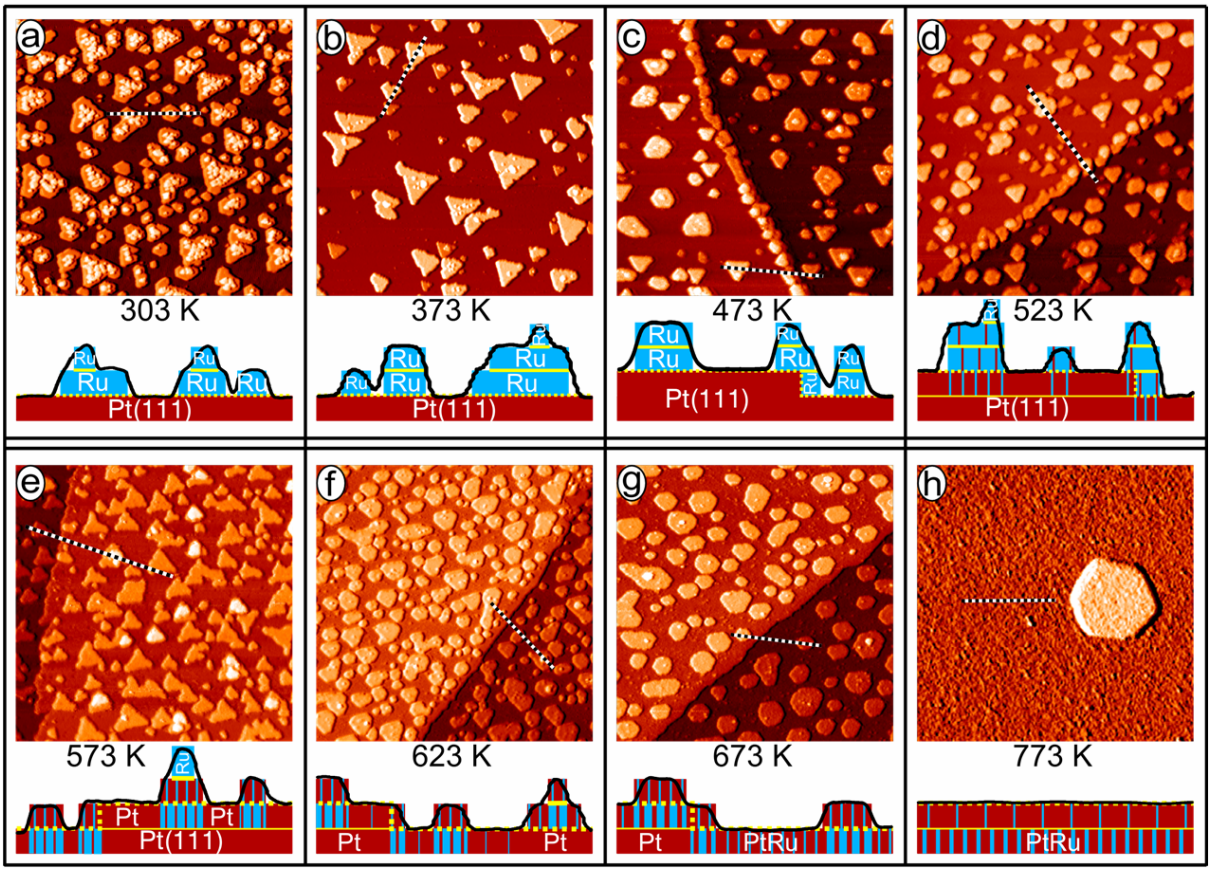

Fig. 6. Representative STM images (100×100 nm^2) recorded after deposition of 0.40±0.04 ML of Ru on a clean Pt(111) surface at different temperatures: a) 303 K; b) 373 K; c) 473 K; d) 523 K; e) 573 K; f) 623 K; g) 673 K, h) 773 K. Height profiles along the black-white dotted lines in the respective STM images are shown together with schematic drawings of the morphology of the islands and the underlying substrate. These also illustrate the chemical composition of the island and the substrate surface layer. Striped patterns indicate (surface) alloy formation and the alloy composition in the respective layer. Reproduced with permission from ref. [25].

In total, Ru_xPt_{1-x}/Pt(111) behaves complementary to Pt_xRu_{1-x}/Ru(0001): the positive segregation energy of Ru in Pt [17,18] favors buried Ru atoms over surface Ru atoms. As on Pt_xRu_{1-x}/Ru(0001), the Ru-rich areas are preferentially overgrown, but now Ru is the guest metal. In other words, Ru_xPt_{1-x}/Pt(111) *surface* alloys are unstable against the formation of Pt/ Ru_xPt_{1-x}/Pt(111) *near-surface* alloys.

2.3 Atom distribution in surface alloys

Visual inspection of the atomically resolved STM data in Figs. 2 and 5 already suggests that the atom distribution in surface alloys varies strongly with the metal combination. Specifically, Pt_xRu_{1-x}/Ru(0001) is characterized by a large number of unlike neighborhoods, whereas equal neighborhoods appear to be favored for Pd_xRu_{1-x}/Ru(0001). In Fig. 7, we give an overview about the atom distributions in five different surface alloys, together with an analysis of the short-range order (SRO) and the underlying effective pair interactions (EPI) [27]. The SRO parameters $\alpha(r)$ are calculated via [28]

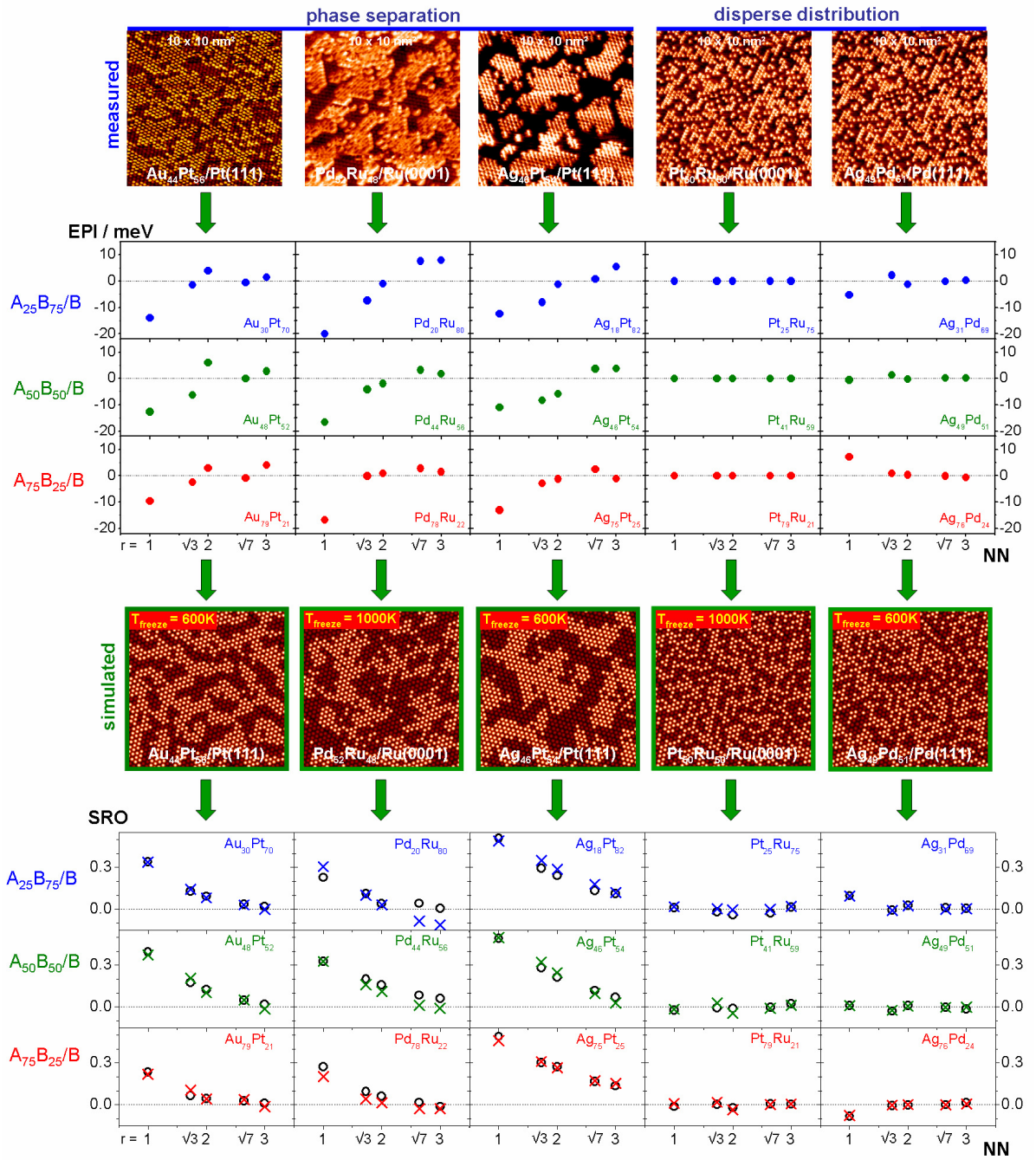

Fig. 7. Measured and simulated atom distribution in five different surface alloys. From left to right: Au_xPt_{1-x}/Pt(111), Pd_xRu_{1-x}/Ru(0001), Ag_xPt_{1-x}/Pt(111), Pt_xRu_{1-x}/Ru(0001), and Ag_xPd_{1-x}/Pd(111). From top to bottom: atomically resolved STM images, effective pair interactions derived from the experimental data, simulated atom distributions, measured and simulated short-range order.

$$\alpha(r) = 1 - p_{AB}(r)/x_B \quad , \tag{1}$$

where $p_{AB}(r)$ and x_B denote the probability to find an atom of type B in a distance r to an atom of type A and the total fraction of B surface atoms, respectively. They are determined directly from atom distributions in STM images or in MC simulations. We calculated $\alpha(r)$ for r = 1, $\sqrt{3}$, 2, $\sqrt{7}$, and 3, with r given in units of the nearest-neighbor (NN) distance. In a random

distribution, $\alpha(r)$ would be zero, whereas positive and negative values of $\alpha(r)$ reflect higher and lower numbers of like neighbors in a distance of r.

Based on the EPI parameters V_{ij}, the total energy of a given atom distribution is approximated by a 2D lattice gas Hamiltonian of the form

$$H = \frac{1}{2}\sum_{i,j} V_{ij} S_i S_j , \qquad (2)$$

where the occupation numbers S_i and S_j at sites i and j, respectively, can assume the values +1 and -1. The EPI parameters V_{ij} only depend on the distance r between these two atoms, $V_{ij} = V_{ij}(r)$. For a 2D lattice occupied by either A (S=-1) or B (S=1) atoms, these parameters are related to the interaction potentials $V^{AA}(r)$, $V^{BB}(r)$, and $V^{AB}(r) = V^{BA}(r)$ via the equation [29]

$$V(r) = ½ (V^{AA}(r) + V^{BB}(r)) – V^{AB}(r). \qquad (3)$$

V(r) thus reflects the energy difference between an equal and an unequal pair of atoms separated by a distance r. (More specifically, the average of the two different equal pairs is taken.) The EPI parameters plotted in Fig. 7 are fitted to the experimental data by loops of systematic parameter variations and tentative MC simulations, until a sufficiently high agreement between measured and simulated SRO is attained [27]. The temperatures used in the MC-simulations (T_{freeze}) are the lowest temperatures for which atom intermixing was observed in the experiments. Though there is no direct analytic relation between the SRO coefficients and the EPIs, one usually observes negative V(1) values for positive $\alpha(1)$ and vice versa. The systems Au_xPt_{1-x}/Pt(111), Pd_xRu_{1-x}/Ru(0001), and Ag_xPt_{1-x}/Pt(111) tend to separate into larger clusters, whereas the distribution in Pt_xRu_{1-x}/Ru(0001) and Ag_xPd_{1-x}/Pd(111) is rather disperse. The distribution in Pt_xRu_{1-x}/Ru(0001) is so close to a random one ($\alpha(r) \approx 0$ for all r), that a simulation with all EPIs set to zero yields sufficient agreement with the experiment. Apart from Ag_xPd_{1-x}/Pd(111), all trends towards either clustering or dispersion agree with ab-initio based predictions for the respective systems [18]. For Ag_xPd_{1-x}/Pd(111), we find a opposite behavior for high and low Ag contents, where the system tends towards clustering and dispersed distributions, respectively. All ‘phase separating’ systems on the left-hand side of Fig. 7 belong to a generic class of bimetallic systems where a pronounced size mismatch of the two components is responsible for a bulk miscibility gap, but at the same time acts as driving force for surface alloy formation (see ref. [30]). For all systems in Fig. 7, the adlayer metal atoms are significantly larger in size than the substrate atoms, leading to compressive strain. This results in an effective repulsion between neighboring guest atoms [30]. This effective repulsion may be changed when including also other effects such as the chemical interaction between the different surface species [30]. Together with the counteracting tensile strain generally present in surface layers, this favors dissolution of the admetal islands and incorporation of the admetal atoms into the outermost substrate layer (‘intermixing’) [31]. The reduction of surface strain by incorporation of larger guest atoms into the host surface layer is also relevant for the tendency towards surface enrichment of these guest metal atoms (see Fig. 5), in addition to possible differences in the metal specific surface energies [32]. It should be noted that this direction of size mismatch seems to be a prerequisite for the stabilization of

surface confined alloys. We are not aware of any experimentally studied surface alloy system where a *smaller* guest atom is stable against bulk dissolution in the host.

2.4 Ab-initio based Monte-Carlo simulations

In this section, we will compare theoretical predictions and experimental results about the nm-scale structure and adsorption behavior of Pt_xAu_{1-x}/Pt(111) surface alloys. Using density functional theory, we have calculated the total energies for 41 periodically repeated structures with Au contents in the range $0.11 \leq x_{Au} \leq 0.89$. We used these data set to calculate pairwise interaction energies (2) via a least-squares fit, which in turn served as input parameters in MC simulations [27]. As illustrated in Figs. 8a and 8b, the agreement between simulated and measured atom distribution is similarly good for ab-initio based as for experiment based EPIs (Fig. 7, left column). As a probe for the chemical properties, we have calculated and measured the adsorption behavior of CO on Pt_xAu_{1-x}/Pt(111). Fig. 9 shows the DFT based adsorption energies of CO on Pt(111), $Au_{0.33}Pt_{0.66}$/Pt(111), $Au_{0.66}Pt_{0.33}$/Pt(111), and on a Au monolayer on Pt(111). Only on-top sites are considered in this plot. As seen in this plot, the neighborhood of Au atoms strengthens the CO adsorption to Pt by about 0.1 eV via an electronic ligand effect, which is partially counterbalanced by a compressive strain effect due to the larger size of the Au atoms, as also found for Pt_xAu_{1-x}/Au(111) surface alloys [33,34]. The Au atoms themselves, however, would adsorb CO only at very low temperatures. Hence, Au_xPt_{1-x}/Pt(111) surface alloys can be characterized as Pt(111) surfaces diluted by non-adsorbing Au atoms, and with a preference for CO adsorption at Pt atoms with one or more Au neighbors. To describe the behavior of CO adlayers with higher coverage, we also considered pairwise CO-CO interactions according to the model proposed in ref [35] for CO on Pt(111). As in the cited paper, we only allow CO adsorption on on-top

a)

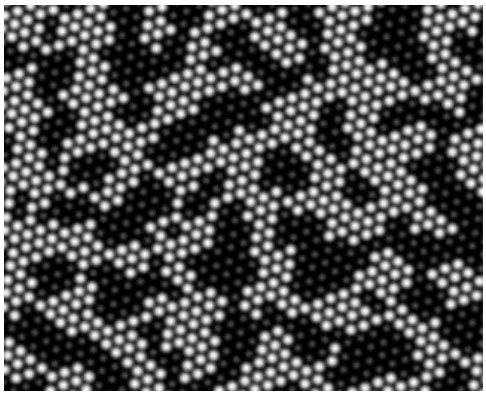

b)

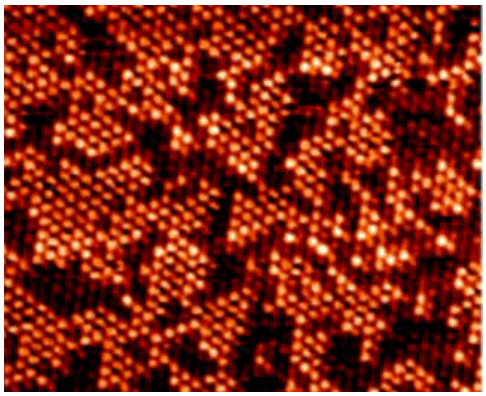

Fig. 8 a) ab-initio MC simulated and b) STM imaged atom distribution in a $Au_{0.44}Pt_{0.56}$ / Pt(111) surface alloy. Au = dark, Pt =

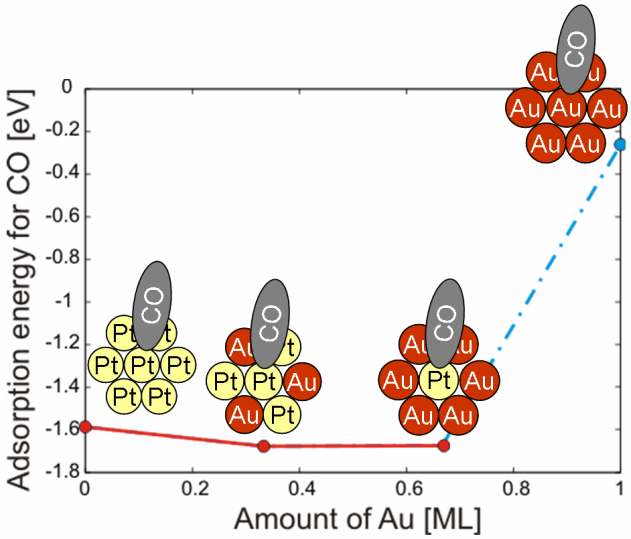

Fig. 9. DFT calculated CO adsorption energies on Pt(111), $Au_{0.33}Pt_{0.66}$/Pt(111), $Au_{0.66}Pt_{0.33}$/Pt(111), and an Au monolayer on Pt(111).

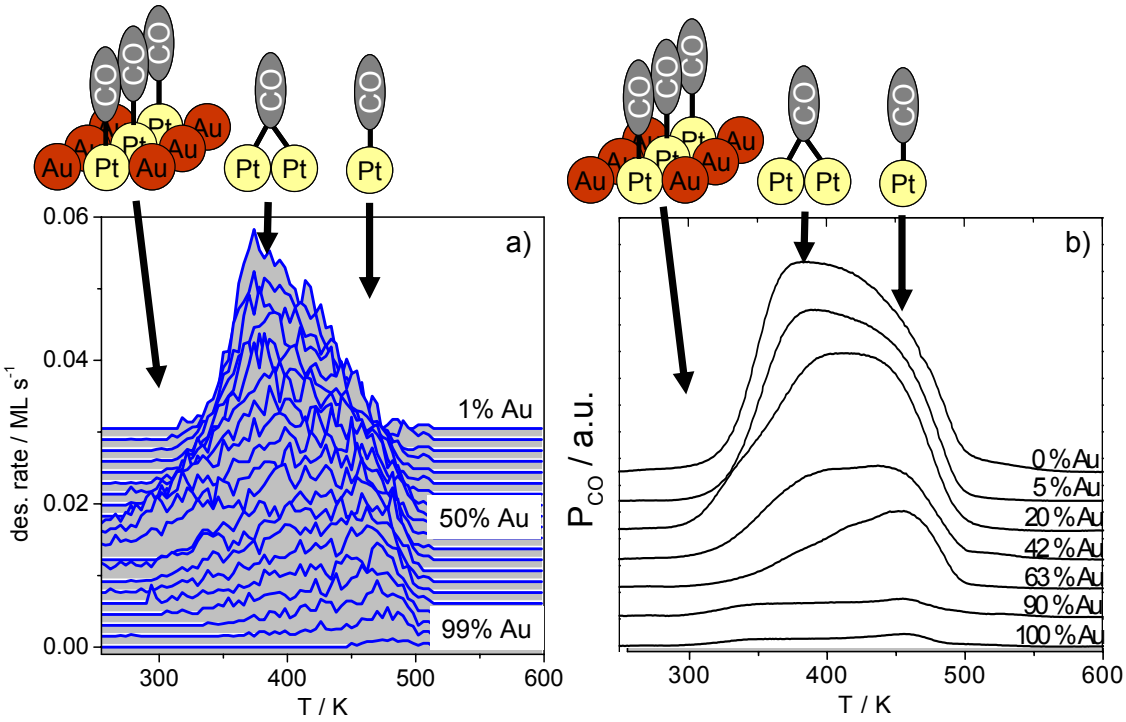

Fig. 10. Thermal desorption spectra of CO on Pt_xAu_{1-x} / Pt(111) surfaces with increasing Au content a) generated by kinetic MC simulations on MC simulated Pt_xAu_{1-x}/Pt(111), and b) measured.

and on bridge sites. The resulting lattice-gas system was used to simulate the distribution of various CO coverages on simulated Pt_xAu_{1-x}/Pt(111) surfaces with varying Au content. In addition to the relaxation of the CO adlayer, we also calculated ensemble averages of the thermal desorption rate, which allowed us to simulate thermal desorption spectra of CO on the simulated surface alloys. The spectra simulated for CO adlayer saturation at increasing Au content of the surface alloys and the corresponding experimental results are shown in Figs. 10c and 10d, respectively. As illustrated in these figures, the ab-initio based simulations helped us understanding the reason for the lower onset of thermal desorption at intermediate Au coverage: the increased stability of CO at Pt due the ligand effect introduced by Au neighbors in combination with the fact that no CO adsorbs on Au gives rise to the formation of chains of CO molecules on rows of Pt atoms that are close to Au patches. These chains actually reflect an 'overpopulation' of the available Pt sites, where the single CO molecule is less stable than in a relaxed CO adlayer on Pt(111). This destabilization arises from repulsion between the two CO nearest-neighbors in such a chain, and it leads to desorption at slightly lower temperatures.

2.5 Nanostructure effects in CO electrooxidation

Alloys consisting of Pt and Ru are known as good electrocatalysts for the electrochemical oxidation of CO, which is an important reaction in low-temperature fuel cells [36,37]. The alloys have a higher activity than either of the pure metals. This is attributed to a combination of alloying-induced changes in the (local) adsorption properties and a bifunctional mechanism, where CO and OH are adsorbed on neighboring Pt and Ru sites, respectively, and have a low barrier for the formation of CO_2. It is generally accepted that the high affinity of Ru to oxygen containing species plays a key role in the high activity of PtRu electrodes [36,37], but many details about the actual interplay of the two metals and the role of the electrode nanostructure are still under debate.

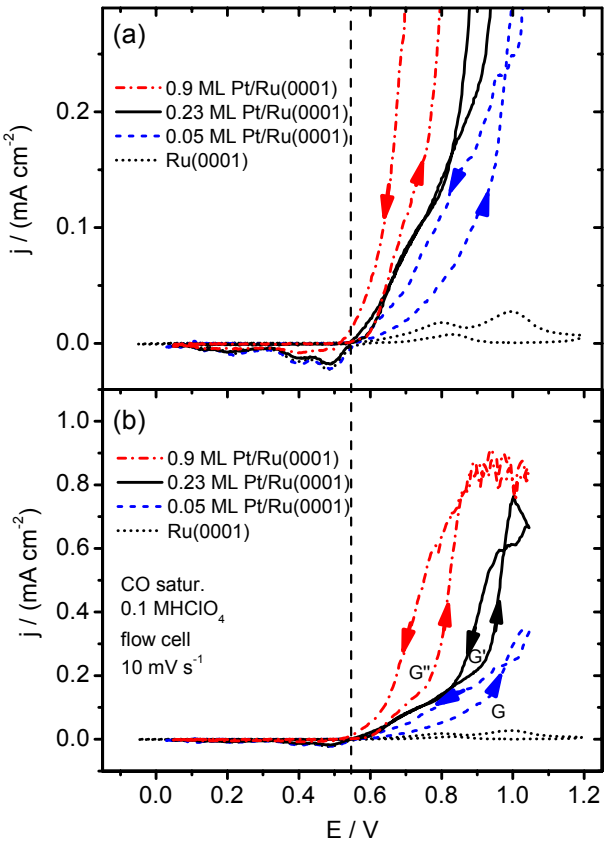

Fig. 11. CO bulk electrooxidation at Ru(0001) and Ru(0001) modified by 0.05, 0.25, and 0.9 ML Pt, measured with 10 mV s^{-1} in flow cell with CO saturated electrolyte (0.1 M $HClO_4$). a) expanded current scale to visualize the onset behavior; b) entire current region. Reproduced with permission from ref. [14]

We have gained some insights into this issue by comparing the CO oxidation behavior of Pt island modified Ru(0001) to that of Pt_xRu_{1-x}/Ru(0001) surface alloys (see Fig. 2). Fig. 11 gives an overview of the potentiodynamic CO oxidation at bare and Pt island modified Ru(0001). As obvious from the low oxidation currents attainable at Ru(0001), this surface itself is totally inactive towards CO oxidation. This drastically changes when small amounts of Pt islands are added to the surface. As on bare Ru(0001), CO oxidation sets in at 0.55 V, but now we observe much higher positive currents. In Fig. 12, we draw the mechanism that we believe is responsible for the enhancement effect by the Pt islands. At 0.55 V, the Ru(0001) surface is covered by a mixture of CO and OH, which due to their strong adsorption to Ru(0001) are not reactive towards CO_2

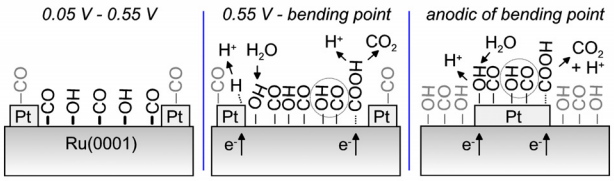

Fig. 12. Illustration of CO electrooxidation at Pt modified Ru(0001); left part: mixed, non-reactive adlayer; middle part: Pt assisted formation of OHad at high local adsorbate coverages on the Ru areas; right part: CO oxidation at the Pt islands. For simplicity, H^+ is used instead of H_3O^+. Reproduced with permission from ref. [14].

formation. At higher potentials, the surface gets increasingly covered with OH from H_2O dissociation. The higher overall coverage increases the adsorbate-adsorbate repulsion and thus reduces their stability. This goes along with a decreased reaction barrier for CO_2 formation ('Brønstedt-Polanyi-Evans' relation [38]). On bare Ru(0001), the H_2O dissociation is hindered by the densely packed adlayer, which explains the low oxidation current on that surface.

Pt monolayer islands on Ru(0001) are known to have a much weaker interaction with adsorbates like O, OH, or CO [4,39,40]. Their adsorbate coverage under reaction conditions should thus be rather low, and species adsorbed there should have a high reactivity. As illustrated in Fig. 12 (middle), we suggest that Pt islands assist in the H_2O dissociation process via a homolytic mechanism, i.e., via temporary adsorption of H_{ad}, which is quickly oxidized towards H^+. In addition, CO can access the surface more easily via the Pt islands than by incorporation into the densely packed and strongly bound, OH_{ad} dominated adlayer on the Ru areas that is formed at higher potentials. Together, this explains why the CO oxidation above 0.55 V is much faster with than without Pt islands [14]. Only at potentials higher than the bending points marked as G, G', and G'' in Fig. 11, the entire process of CO oxidation predominantly takes place on the Pt islands.

The CO oxidation activity is further enhanced when going from Pt modified Ru(0001) to dispersed Pt_xRu_{1-x}/Ru(0001) surface alloys (Fig. 13, see also Fig. 2). At low Pt content, CO oxidation sets in at 0.55 V, but now with even higher rates than at the Pt island modified surfaces. At higher Pt contents, the onset potential is shifted to lower potentials, which indicates an intrinsically higher electrocatalytic activity of such surfaces. We suggest that

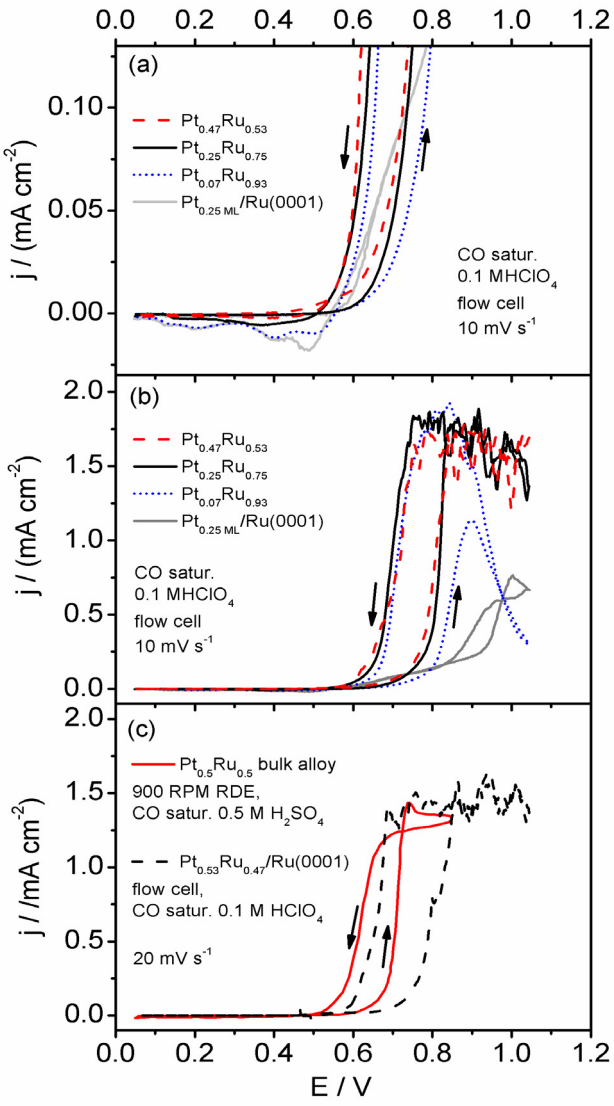

Fig. 13. CO bulk electrooxidation at PtRu alloys. a) and b): Pt_xRu_{1-x}/Ru(0001) (x=0.07, 0.25, 0.47) surface alloys measured in flow cell with CO saturated electrolyte. c) Sputtered $Pt_{0.5}Ru_{0.5}$ bulk alloy in rotating disc electrode setup, (data from ref. [37]), compared to a $Pt_{0.53}Ru_{0.47}$/Ru(0001) surface alloy. Reproduced with permission from ref. [14]

this enhancement results from the availability of adsorption sites with a bonding power in-between those of the strongly binding Ru(0001) surface and the weakly adsorbing Pt monolayers on Ru(0001). On such a surface, fewer contributions from adsorbate-adsorbate repulsion are needed to reduce the stability of the adsorbates and thus the activation energy for CO_2 formation. Gradual variations of adsorption energies result from the local interplay of Pt and Ru atoms via ligand and mixed-ensemble effects. As illustrated in Fig. 13c, the potential-dependent CO oxidation at the surface alloys shows trends that are similar to previous findings for PtRu bulk alloys, which underlines the importance of sub-nm scale dispersion for the high performance of PtRu catalysts [14].

3 Conclusions

Surface alloys of the type A_xB_{1-x}/B formed of a guest metal A and a host metal B on close-packed surfaces of metal B are interesting and well-defined model systems for fundamental studies of adsorption and reaction at bimetallic surfaces. Thermodynamically, surface alloys reflect a local minimum in free energy, i.e., they are metastable with respect to bulk dissolution. In particular, they are more stable than foreign metal islands, which are transformed into surface alloys at sufficiently high temperatures. The transformation takes places by a combination of adatom diffusion and exchanges between adatoms and substrate atoms. When the segregation energy of the guest metal is sufficiently negative, overgrowth of guest metal atoms is unfavorable, which stabilizes the surface alloy in the outermost surface layer. Otherwise, the *surface alloy* is rather buried by the host metal and thus transformed into a *near-surface* alloy.

Surface alloys and near-surface alloys can both be formed in a temperature range where adatom diffusion and place exchanges between adatoms and substrate atoms are possible, but bulk diffusion is still hindered. This kinetic stabilization is responsible for the metastable character of the surface alloys, which is also important for their stability in adsorption and reaction experiments.

Surface alloys thus are in a local equilibrium, which allows describing the lateral atom distributions by thermodynamic concepts. Due to the high temperatures needed for surface intermixing, surface alloys usually do not exhibit long-range but only short-range order. Using additive interaction energies, the nm-scale distributions can be simulated in a Metropolis Monte-Carlo approach. The input parameters can be attained by fitting to either experimental or theory data. Simulated surface alloys can in turn be used to simulate the interaction of adsorbates with these surfaces. As an example, we have shown simulated thermal desorption of CO from simulated $Au_xPt_{1-x}/Pt(111)$ surface alloys, which helped understanding the trends in the corresponding experimental data.

Electrochemical CO oxidation measurements at well-defined model surfaces have highlighted the importance of sub-nm scale dispersion for the electrocatalytic activity of PtRu electrodes. The atomic scale intermixing provides a high versatility of adsorption sites with intermediate

bonding power, which according to the Sabatier principle is beneficial for the catalytic activity of a catalyst system.

Acknowledgements

This work was supported by the “Landesstiftung Baden-Württemberg” via the “Kompetenz-netz Funktionelle Nanostrukturen” (project B12). O.B. Alves is grateful for financial support by the “Deutscher Akademischer Austauschdienst”

References

[1] J. H. Sinfelt in: Bimetallic Catalysts: Discoveries, Concepts and Applications, (Wiley, New-York, 1983).

[2] C. T. Campbell: in Handbook of Heterogeneous Catalysis, Edited by G. Ertl, H. Knözinger, and J. Weitkamp (Wiley-VCH, Weinheim, 1997), Vol. 2.

[3] M. Mavrikakis, B. Hammer, and J. K. Nørskov, Phys Rev Lett 81, 2819 (1998).

[4] A. Schlapka, M. Lischka, A. Gross, U. Käsberger, and P. Jakob: *Surface Strain versus Substrate Interaction in Heteroepitaxial Metal Layers: Pt on Ru(0001)*, Phys Rev Lett 91, 016101 (2003).

[5] A. Gross: *Reactivity of bimetallic systems studied from first principles*, Top Catal 37, 29 (2006).

[6] A. Gross: *Adsorption at nanostructured surfaces from first principles*, J Comput Theoret Nanosci 5, 894 (2008).

[7] W. M. H. Sachtler: in Handbook of Heterogeneous Catalysis, Edited by G. Ertl, H. Knözinger, and J. Weitkamp (VCH-Wiley, Weinheim, 1997), Vol. 3.

[8] Y. Soma-Noto and W. M. H. Sachtler, J Catal 34, 162 (1974).

[9] S. Sakong, C. Mosch, and A. Gross: *CO adsorption on Cu-Pd alloy surfaces: ligand versus ensemble effects*, Phys Chem Chem Phys 9, 2216 (2007).

[10] P. T. Wouda, B. E. Nieuwenhuys, M. Schmid, and P. Varga, Surf Sci 359, 17 (1996).

[11] B. Gleich, M. Ruff, and R. J. Behm: *Correlation between local substrate structure and local chemical properties: CO adsorption on well-defined bimetallic Au/Pd(111) surfaces*, Surf Sci 386, 48 (1997).

[12] M. Ruff, N. Takehiro, P. Liu, J. K. Norskov, and R. J. Behm: *Size-specific chemistry on bimetallic surfaces: a combined experimental and theoretical study*, ChemPhysChem 8, 2068 (2008).

[13] F. Maroun, F. Ozanam, O. M. Magnussen, and R. J. Behm: *The role of atomic ensembles in the reactivity of bimetallic electrocatalysts*, Science 293, 1811 (2001).

[14] H. E. Hoster and R. J. Behm: *The Effect of Structurally well-defined Pt Modification on the Electrochemical and Electrocatalytic Properties of Ru(0001) Electrodes*, in Fuel Cell Catalysis: A Surface Science Approach, Edited by M. T. M. Koper (Wiley&Sons, Chichester, 2008), Chap. 14.

[15] B. Hammer and J. K. Nørskov, Adv Catal 45, 71 (2000).

[16] E. Christoffersen, P. Liu, A. Ruban, H. L. Skriver, and J. K. Nørskov, J Catal 199, 123 (2001).

[17] A. V. Ruban, H. L. Skriver, and J. K. Nørskov, Phys Rev B 59, 15 990 (1999).

[18] A. Christensen, A. V. Ruban, P. Stoltze, K. W. Jacobsen, H. L. Skriver, J. K. Nørskov, and F. Besenbacher, Phys Rev B 56, 5822 (1997).

[19] H. E. Hoster, A. Bergbreiter, P. Erne, T. Hager, H. Rauscher, and R. J. Behm: *Atom distribution in well-defined Pt_xRu_{1-x}/Ru(0001) monolayer surface alloys*, Phys Chem Chem Phys 10, 3812 (2008).

[20] F. Buatier de Mongeot, M. Scherer, B. Gleich, E. Kopatzki, and R. J. Behm: *CO Adsorption and Oxidation on Bimetallic Pt/Ru(0001) Surfaces - A Combined STM and TPD/TPR Study*, Surf Sci 411, 249 (1998).

[21] T. Diemant, T. Hager, H. E. Hoster, H. Rauscher, and R. J. Behm: *Hydrogen adsorption and coadsorption with CO on well-defined bimetallic PtRu surfaces – A model study on the CO tolerance of bimetallic PtRu anode catalysts in low temperature Polymer Electrolyte Fuel Cells* , Surf Sci 541, 137 (2003).

[22] H. Hartmann, T. Diemant, A. Bergbreiter, J. Bansmann, H. Hoster, and R. J. Behm: *Surface alloy formation, short-range order, and deuterium adsorption properties of monolayer PdRu/Ru(0001) surface alloys*, Surf Sci **603,** 1456 (2008).

[23] H. Hartmann, T. Diemant, J. Bansmann, and R. J. Behm: *Chemical properties of structurally well-defined PdRu/Ru(0001) surface alloys - Interaction with CO*, Surf Sci **603,** 1439 (2008).

[24] A. Bergbreiter, H. E. Hoster, and R. J. Behm: *Floating PtRu and PdRu surfacea alloys on Ru(0001),* in preparation.

[25] A. Berkó, A. Bergbreiter, H. E. Hoster, and R. J. Behm: *From bilayer to monolayer growth: Temperature effects in the growth of Ru on Pt(111)*. Surf Sci (2009), doi.org/10.1016/j.susc.2009.05.033.

[26] A. Bergbreiter, A. Berkó, P. M. Erne, H. E. Hoster, and R. J. Behm: *On the Origin of Ru Bilayer Island Growth on Pt(111)*, Vacuum (2009), doi.org/10.1016/j.vacuum.2009.04.001.

[27] A. Bergbreiter, H. E. Hoster, S. Sakong, A. Gross, and R. J. Behm: *Energetics driving the short-range order in Cu_xPd_{1-x}/Ru(0001) monolayer surface alloys*, Phys Chem Chem Phys **9,** 5127 (2007).

[28] S. Müller, J Phys : Condens Matter **15,** R1429 (2003).

[29] A. V. Ruban, H. L. Skriver, and J. K. Nørskov, in *Surface Alloys and Alloy Surfaces*, Edited by D. P. Woodruff (Elsevier; Amsterdam, 2002), Vol. 10.

[30] J. Tersoff, Phys Rev Lett **74,** 434 (1995).

[31] M. Schmid, W. Hofer, P. Varga, P. Stoltze, K. W. Jacobsen, and J. K. Nørskov, Phys Rev B **51,** 10937 (1995).

[32] L. Vitos, A. V. Ruban, H. L. Skriver, and J. Kollár, Surf Sci **411,** 186 (1998).

[33] Y. Gohda and A. Gross: *Local reactivity of ultrathin platinum overlayers and surface alloys on a gold surface*, Surf Sci **601,** 3702 (2009).

[34] Y. Gohda and A. Gross: *Structure-reactivity relationships for bimetallic electrodes: Pt overlayers and PtAu surface alloys on Au(111)*, J Electroanal Chem **607,** 47 (2007).

[35] J.-S. McEwen, S. H. Payne, H. J. Kreuzer, M. Kinne, R. Denecke, and H.-P. Steinrück, Surf Sci **545,** 47 (2003).

[36] M. Watanabe and S. Motoo, J Electroanal Chem **60,** 275 (1975).

[37] H. A. Gasteiger, N. M. Markovic, and P. N. Ross, J Phys Chem **99,** 8290 (1995).

[38] N. Bronstedt, Chem Rev **5,** 231 (1928).

[39] M. Lischka, C. Mosch, and A. Gross: *Tuning catalytic properties of bimetallic surfaces: Oxygen adsorption on pseudomorphic Pt/Ru overlayers*, Electrochim Acta **52,** 2219 (2007).

[40] M. T. M. Koper, T. E. Shubina, and R. A. van Santen, J Phys Chem B **106,** 686 (2002).